

# Fan-Beam Reconstruction Under Motion and Data Truncation: Comparing Analytic and Iterative Approaches

Jan Hoskovec, Fabien Momey, Rolf Clackdoyle, Laurent Desbat and Simon Rit

**Abstract**—In this paper, we compare analytic and iterative fan-beam reconstruction approaches when the object undergoes some rigid motion during the scan, and in the situation of truncated projections. Based on our recent work presenting an exact analytic reconstruction method for this problem, we are able to predict the field of theoretically reconstructible points for our method. The object motion is handled by using a reference frame attached to the object, which therefore appears static while the source trajectory undergoes a non-circular “virtual” motion. We implemented the iterative reconstruction as the convex minimization of a data-fidelity term under non-negativity constraint and regularization to solve this static problem with virtual source trajectory. We compared the reconstructed field of view for the two methods on 2D fan-beam Shepp-Logan phantom simulations. Our results show that both methods validate the predicted reconstructible zone and correlate well in terms of reconstruction quality. The iterative reconstruction also demonstrates that in certain cases it is possible to recover structures beyond the strict analytic frontier of reconstructibility.

**Index Terms**—Tomography, Region-Of-Interest Tomography, Dynamic Tomography.

## I. INTRODUCTION

In [1], we reported on a method for performing exact analytic 2D fan-beam reconstruction when the object of interest has undergone a perfectly known rigid translation during the circular scan, also involving data truncation. Rigid object motion transforms the circular source trajectory into a virtual one which can involve data truncation. The method exploits the data redundancy from the  $2\pi$  source trajectory to extend the field of reconstructible points where Differentiated Back-Projection with Hilbert filtering (DBP-H) [5] can be performed. The algorithm was tested in a proof-of-concept study on Shepp-Logan phantom simulations with several motion cases and detector sizes.

In this paper, we compare the results given by our analytic algorithm with an iterative reconstruction approach, particularly in terms of the predicted field of reconstructible points. Our results from Shepp-Logan phantom simulations show a very good match regarding the almost perfectly reconstructed zone of the phantom, and highlight possibilities for the iterative method to reconstruct beyond the predicted field of view.

## II. MATERIALS AND METHODS

### A. Geometry

Our work takes place in the context of 2D fan-beam reconstruction from a circular scan around the object. The geometry is illustrated

This work was supported by the DROITE project (Dynamic ROI tomography, Theory and Experiments), funded by the French ANR (N° ANR-12-BS01-0018).

Jan Hoskovec is with Laboratoire Hubert Curien : CNRS UMR 5516, Saint-Étienne, France and with CREATIS ; CNRS UMR 5220 ; INSERM U 1044, Lyon, France, and was supported by an Allocation de Recherche from la Région Rhône-Alpes. E-mail: jan.hoskovec@univ-st-etienne.fr

Fabien Momey is with TIMC-IMAG ; CNRS UMR 5525, Grenoble, France

Rolf Clackdoyle was with Laboratoire Hubert Curien, is now with TIMC-IMAG ; CNRS UMR 5525, Grenoble, France

Laurent Desbat is with TIMC-IMAG ; CNRS UMR 5525, Grenoble, France

Simon Rit is with CREATIS ; CNRS UMR 5220 ; INSERM U 1044, Lyon, France

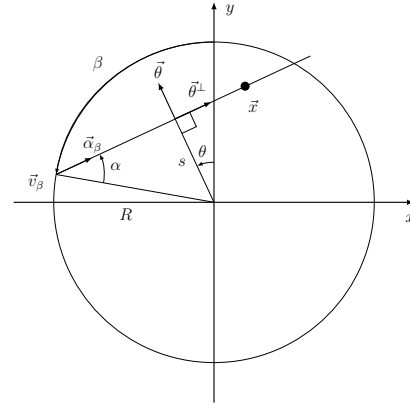


Fig. 1. The fan-beam projection geometry. The source is at  $\vec{v}_\beta$  and the trajectory radius is  $R$ . A measured ray in the fan-beam geometry is parametrized by  $(\alpha, \beta)$ . Also shown are the equivalent parameters  $(s, \theta)$  expressing the same ray in the parallel projection geometry.

in Fig.1. Fan-beam projections of a density function  $f(\vec{x})$  can be written as:

$$p(\alpha, \beta) = \int_{-\infty}^{\infty} f(\vec{v}_\beta - t\vec{\alpha}_\beta) dt \quad (1)$$

with  $\beta$  the polar angle of the source from the vertical axis and  $\vec{v}_\beta = R\vec{\beta} = R(-\sin \beta, \cos \beta)^T$  the source position. The fan angle is denoted  $\alpha$  and  $\vec{\alpha}_\beta = (-\sin(\alpha + \beta), \cos(\alpha + \beta))^T$  is the direction of the ray emanating from the source. The angular conventions taken here are illustrated Fig. 1.

Fan-beam data  $p(\alpha, \beta)$  can be related to equivalent parallel-beam projections  $\bar{p}(s, \theta)$  via the following change of variables:

$$\theta = \alpha + \beta - \frac{\pi}{2} \quad (2)$$

$$s = R \sin \alpha, \quad (3)$$

therefore

$$p(\alpha, \beta) = \bar{p}(R \sin \alpha, \alpha + \beta - \frac{\pi}{2}). \quad (4)$$

### B. DBP-H Formula

We summarize here our analytical reconstruction method, which was presented in [1]. This method belongs to the DBP-H family, sometimes called simply DBP, or BPF, for Backprojection-Filtration. More specifically, the DBP-H algorithm used here is of the “backproject first” approach [9], which begins by performing two backprojections of the unprocessed sinogram data onto the target pixel grid. Then, via a simple sum of partial derivatives of each weighted backprojection, we obtain the same Hilbert image of the object of interest as if we had performed a differentiation along the flat detector before backprojecting.

The general DBP-H reconstruction formula is given by

$$H_\phi f(\vec{x}) = \frac{-1}{2\pi} b_\phi(\vec{x}) = \frac{-1}{2\pi} \int_{\phi}^{\phi+\pi} \frac{\partial}{\partial s} \bar{p}(s, \theta) \Big|_{s=\vec{x} \cdot \vec{\theta}} d\theta. \quad (5)$$

where  $H_\phi f$  denotes a 1D Hilbert transform along the vector  $\vec{\phi} = (\cos \phi, \sin \phi)^T$ . With the “backproject first” approach, we obtain  $b_\phi(\vec{x})$  by the following relation (see [1] or [9] for full derivation):

$$\begin{aligned} b_\phi(\vec{x}) &= \frac{\partial}{\partial x} \int_{\phi}^{\phi+\pi} \bar{p}(\vec{x} \cdot \vec{\theta}, \theta) (-\sin \theta) d\theta \\ &\quad + \frac{\partial}{\partial y} \int_{\phi}^{\phi+\pi} \bar{p}(\vec{x} \cdot \vec{\theta}, \theta) (\cos \theta) d\theta \end{aligned} \quad (6)$$

where  $\vec{\theta} = (-\sin \theta, \cos \theta)^T$ .

### 1) Handling motion and truncation for DBP-H reconstruction:

The “backproject first” DBP-H algorithm is useful in the context of motion-compensated reconstruction, since all motion corrections can be included *before* the sinogram data is processed in any manner. Our algorithm from [1] does just that when it rearranges motion contaminated full-scan fan-beam data into an equivalent, static, parallel-beam geometry.

When the object undergoes a (rigid) translation, the sinogram data may become truncated (when part of the object “leaves” the scanner’s field-of-view during the scan). Since a rigid displacement of the object (described by a vector  $\vec{d}_\beta$  parametrized by the gantry angle) is equivalent to a deformation of the X-Ray source trajectory by subtracting the same vector from its physical path, static truncation (due to limited detector width) and dynamic truncation (induced by object motion) can be handled as the same problem.

Observing the virtual trajectory  $\vec{v}_\beta - \vec{d}_\beta$ , we recall that with the DBP-H methods, we can compute a Hilbert image of a point if it is observable from a large enough segment of the (here, virtual) trajectory [5][6][8]. Such a point becomes theoretically reconstructible via (5). We refer to this type of point as a Hilbert point.

Taking advantage of the data redundancy inherent to a full scan, our algorithm can also recover points for which such a segment of the virtual trajectory is not available, but where data from the opposite side of the scan can fill in the gap. See [1] for details.

In practice, to reconstruct the object, we also need to be able to invert the Hilbert transform of the points we obtain. With a small *a priori* about the image support, we can invert Hilbert points using the finite-support Hilbert transform inversion formula from [3] on all line segments of Hilbert points which cross the entire object support. This condition also influences the choice of the angle  $\phi$ .

### C. Iterative reconstruction method for truncated projections and a virtual trajectory

Our iterative reconstruction algorithm looks for the static image  $f$  which minimizes the least squares criterion - the data-fidelity term - under a non-negativity constraint, with a regularization term:

$$\mathbf{f}^+ = \arg \min_{f \geq 0} \left\{ \left\| \mathbf{R}^\beta \cdot \mathbf{f} - \mathbf{p}^\beta \right\|_2^2 + \mu \mathcal{J}_{\text{prior}}(\mathbf{f}) \right\}, \quad (7)$$

where  $\mathbf{p}^\beta = \{\mathbf{p}^{\beta_k} | k = 1 \dots N_\beta\}$  stands for the set of  $N_\beta$  fan-beam projections, and  $\mathbf{R}^\beta$  is the model of fan-beam projections along the virtual (perturbed) source trajectory at the virtual angular positions  $\{\beta_k | k = 1 \dots N_\beta\}$ .

The data-fidelity term ensures consistency of the model with the data. A non-negativity constraint is added as the object to be reconstructed is known to have positive values. The term  $\mathcal{J}_{\text{prior}}$  accounts for prior information. The constraint and the regularizer are necessary for the reconstruction algorithm to effectively converge to a relevant solution, avoiding artifacts amplifications and noise. The hyperparameter  $\mu$  controls the tradeoff between data fitting and regularization.

We chose an edge-preserving smoothness regularizer expressed as a relaxed total variation (TV) prior [7]:

$$\mathcal{J}_{\text{prior}}(\mathbf{f}) = \sum_i \sqrt{\|\nabla_i \cdot \mathbf{f}\|_2^2 + \epsilon^2}, \quad (8)$$

with  $\epsilon > 0$  the relaxation parameter and  $\nabla_i$  a finite difference operator approximating the spatial gradient at position  $i$ .

The minimization of (7) was carried out by the VMLM algorithm [4], a limited memory quasi-Newton method, for which we have added the handling of the non-negativity constraint.

### III. SIMULATIONS AND RECONSTRUCTIONS

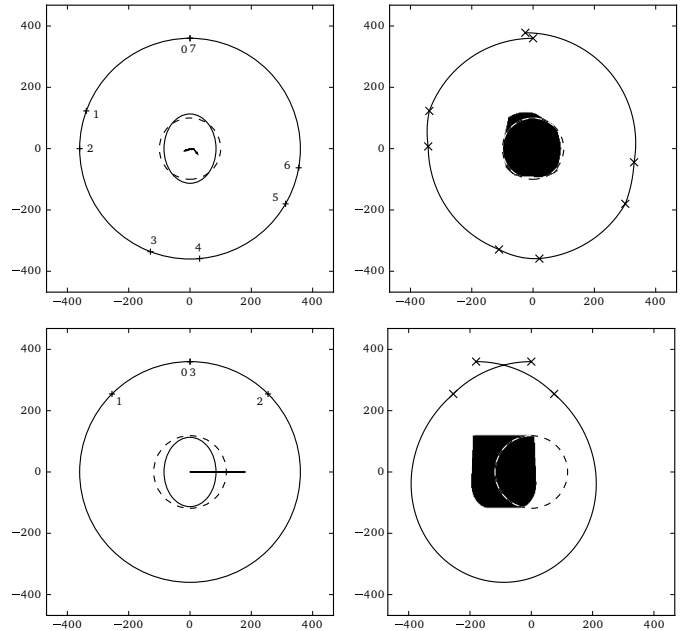


Fig. 2. Top left: Representation of motion 1. Bottom left: Representation of motion 2. Top right and bottom right: virtual trajectory, static FOV and regions of Hilbert points (in black) obtained respectively with the motions 1 and 2.

We simulated the projection data of an off-centered slice of the 3D Shepp-Logan phantom [2] for two cases of rigid motion of the phantom. Each case corresponded to a sequence of constant-velocity translations of the phantom during a circular scan of radius  $R = 360$  mm with a flat detector at 480 mm from the source. *Motion 1* consisted of translations that occurred only during scan intervals  $\beta \in [70^\circ, 90^\circ] \cup [159^\circ, 185^\circ] \cup [240^\circ, 270^\circ]$ , which were respectively translations by vectors  $R(-0.05, -0.02)^T, R(0.08, 0.02)^T, R(0.05, -0.04)^T$ . *Motion 2* consisted of a single translation, occurring during the scan interval  $\beta \in [45^\circ, 315^\circ]$ , by the vector  $R(0.5, 0)^T$ . The rigid motions, as well as the equivalent (“virtual”) source trajectories, are illustrated in Fig.2.

In this study the motion was assumed to be perfectly known, so was the corresponding virtual trajectory. For both methods, we reconstructed an image of  $510 \times 510$  pixels with a sampling rate of 1 mm in both directions.

The analytic method proceeds by first introducing a map of Hilbert points. Its comparison with the *a priori* known phantom support helps to identify convenient Hilbert filtering directions. Once the direction is chosen, the corresponding Hilbert images are generated, and finite Hilbert inversion carried out along Hilbert lines. More details can be found in [1].

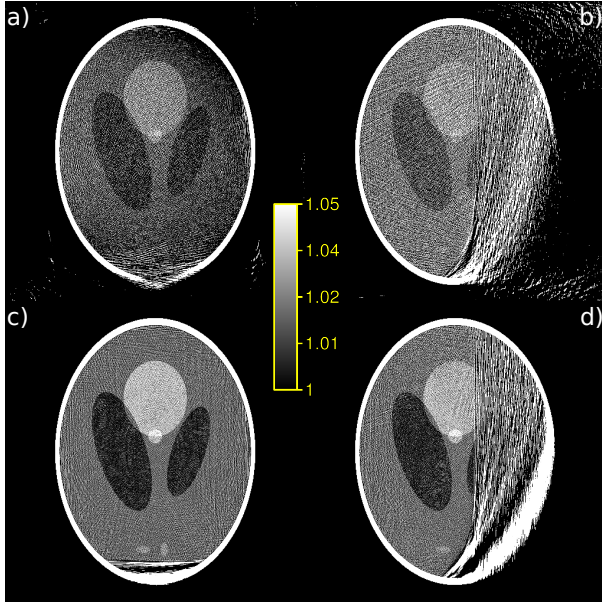


Fig. 3. Reconstructions of simulated cases *motion 1* (first column) and *motion 2* (second column) with the iterative reconstruction method. (a-b) Reconstruction without non-negativity constraint and without regularization. (c-d) Reconstruction with non-negativity constraint and without regularization.

For the iterative reconstruction, the value of  $\epsilon$  was chosen to be  $10^{-3}$ , i.e. 1/10 of the minimum contrast value of the Shepp-Logan phantom. Therefore structures with contrast larger than this value would be preserved in the image, and smoothed otherwise. The hyperparameter  $\mu$  was carefully tuned “by hand” until a satisfactory reconstruction quality was reached. A suitable value found was  $\mu = 10^3$ . The quality of the iterative reconstruction strongly depends on the degree of regularization. In general, a low value of  $\mu$  or no regularization causes errors due to reprojection model approximations and noise amplification. Therefore, it is essential to regularize the solution, and preliminary results tended to verify this claim, as illustrated in Fig. 3 compared to Fig. 4(f)(g). Furthermore, we observed in our reconstructions a dramatic effect of the non-negativity constraint appeared to drive the algorithm to “put the information in the right zones”, see Fig. 3(c)(d) compared to Fig. 3(a)(b).

Fig. 4 shows the reconstructions obtained with both methods. Fig. 5 displays horizontal profiles taken across two different horizontal lines through the phantom.

The analytic reconstructions were accurate in the predicted regions. We recall that the method proposed is mathematically correct for the intersection of the region of Hilbert points with all lines that traverse the (known) support of the object without contracting a non-Hilbert point. For motion 2, a set of Hilbert points not satisfying this condition was easily identified and corresponds to the bright white region of Fig. 4(e). For the reconstructions of motion 1 with horizontal filtering ( $\phi = 0$ ), the profiles in Fig. 5 indicate excellent quantitative reconstruction in the predicted regions (Fig. 4(c)). For reconstructions with an oblique filtering directions (Fig. 4(d)(e)) however, there seemed to be at times a small positive bias related to the difficulties of choosing the right constant for the finite Hilbert inversion, visible as faint light bands along the filtering direction.

For the iterative reconstruction, we immediately note that the effective reconstruction zone stretches beyond the boundary between the theoretically reconstructible and non reconstructible points, even though the error is higher in the zone of uncertainties (cf. Fig. 4(h)(i) and Fig. 5). This behavior is probably due to these regions suffering

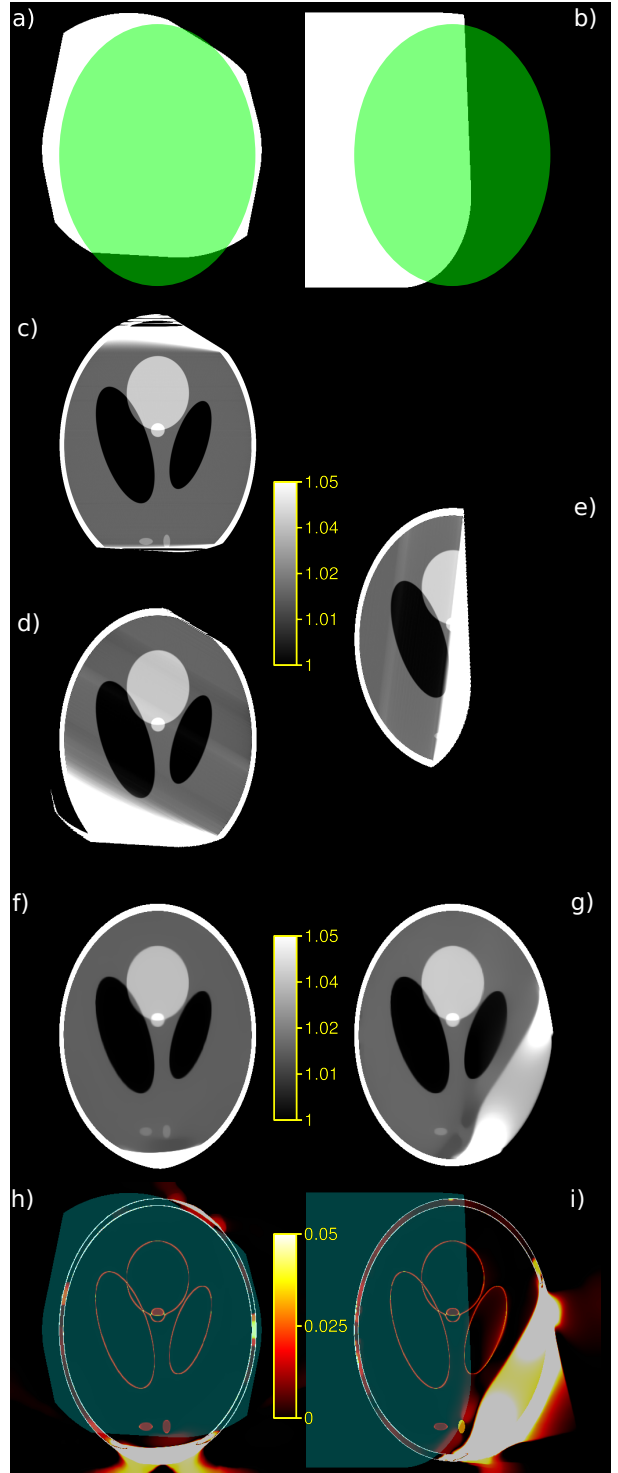


Fig. 4. Reconstructions of simulated cases *motion 1* (first column) and *motion 2* (second column) with both the analytic and iterative reconstructions methods. (a-b) Predicted FOV of reconstructible points. (c-e) Reconstruction with the analytic DBP-H method. (c) and (d) both correspond to motion 1, using different values of  $\phi$ . (f-g) Iterative reconstruction. (h-i) Absolute value of the difference's map between ground truth image and iterative reconstruction, superimposed with the predicted FOV (in cyan).

only small amounts of missing data that prevent an analytic solution. The iterative algorithm was able to recover some structures. We note

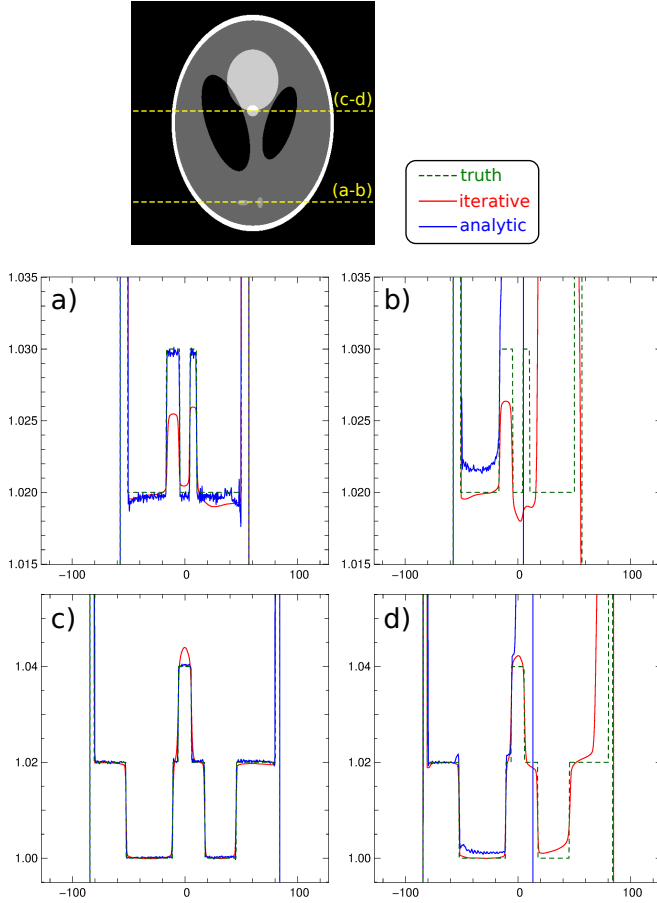


Fig. 5. Profiles taken in the reconstructions of Fig. 4. (a-c) *motion 1*. (b-d) *motion 2*. Note that the vertical scale for (a) and (b) is magnified by nearly 2.5 times compared to the one for (c) and (d).

that the regularization played a strong role here because Fig. 3 showed poor recovery of the iterative algorithm in exactly the “non-Hilbert point” areas of the object. In general, the quality of such extrapolations is strongly object-dependent, and some lines of response can bring more information than others if the structures are oriented in suitable directions. We also notice from the profiles of Fig. 5 that injecting regularization causes some bias in the recovered values of the finer structures even in the areas identified as reconstructible. This can be mitigated by decreasing the value of the hyperparameter  $\mu$ , but at the cost of increasing the variance of reconstruction errors as seen in Fig. 3. Hence the regularization in our experiments showed the usual trade-off between bias and variance of the solution. However, there is no indication in the “non-reconstructible” region which features are correct and which are incorrect. Although, in Fig. 4(g), the large black ellipsoid on the right is correctly recovered, the small white ellipsoid at the bottom is completely missing.

#### IV. DISCUSSION AND CONCLUSION

The results of our simulations show good coherence of the reconstructible regions predicted by the analytic method and the part of the image where the reconstruction by the iterative method was quantitatively successful. The iterative method, however, manages to recover certain features outside that region in a way which is still readable, although great care must be taken with interpreting such features in the non-reconstructible zone.

Our results also showed that the regularization and non-negativity constraint were essential for the iterative reconstruction to produce a good trade-off between bias and variance.

The analytic method’s potential was constrained by the need to have Hilbert points aligned on a segment crossing the object support entirely in order to be able to recover that part of the image. Implementing an iterative one-sided Hilbert transform inversion method alongside the analytic backprojection could lead to a reconstruction method where the whole reconstructible region is recovered.

#### REFERENCES

- [1] J. Hoskovec, R. Clackdoyle, L. Desbat and S. Rit. *Exact fan-beam reconstruction with arbitrary object translations and truncated projections*. To appear in: IEEE Trans. Nucl. Sci., 2016.
- [2] A.C. Kak and M. Slaney. *Principles of Computerized Tomographic Imaging*. Piscataway, NJ, 1988.
- [3] S.G. Michlin and A.H. Armstrong. *Integral equations and their applications to certain problems in mechanics, mathematical physics and technology*. London, 1957.
- [4] J. Nocedal. *Updating quasi-Newton matrices with limited storage*. Mathematics of computation, vol. 35, no. 151, pp. 773–782, 1980.
- [5] F. Noo, R. Clackdoyle, and J.D. Pack. *A two-step Hilbert transform method for 2D image reconstruction*. Phys. Med. Biol., vol. 49, no. 17, p. 3903, 2004.
- [6] J.D. Pack, F. Noo, and R. Clackdoyle. *Cone-beam reconstruction using the backprojection of locally filtered projections*. IEEE Trans. Med. Imag., vol. 24, no. 1, pp. 70–85, 2005.
- [7] L.I. Rudin, S. Osher and E. Fatemi. *Nonlinear total variation based noise removal algorithms*. Physica D: Nonlinear Phenomena, vol. 60, no. 1, pp. 259–268, 1992.
- [8] D. Xia, E. Sidky, L. Yu, Y. Zou, and X. Pan. *Exact ROI image reconstruction with perturbed source trajectories in C-arm CT*. Nuclear Science Symp. Conf. Rec., vol. 4. IEEE, 2005, pp. 4–pp.
- [9] G.L. Zeng. *Image reconstruction via the finite Hilbert transform of the derivative of the backprojection*. Med. Phys., vol. 34, no. 7, pp. 2837–2843, 2007.